Generation of temporal multimode squeezed states of femtosecond pulse light

Chihua Zhou (周驰华)[1,2], Changchun Zhang (张长春)[1,2], Hongbo Liu (刘宏波)[1,2], Kui Liu (刘 奎)[1,2,*], Hengxin Sun (孙恒信)[1,2], and Jiangrui Gao (郜江瑞)[1,2]

[1]*State Key Laboratory of Quantum Optics and Quantum Optics Devices, Institute of Opto-Electronics, Shanxi University, Taiyuan 030006, China*

[2]*Collaborative Innovation Center of Extreme Optics, Shanxi University, Taiyuan 030006, China*

**Corresponding author: liukui@sxu.edu.cn*

Received January 22, 2017; accepted May 23, 2017; posted online June 23, 2017

Nonclassical optical frequency combs play essential roles in quantum computation in the continuous variable regime. In this work, we generate multimode nonclassical frequency comb states using a degenerate type-I synchronously pumped optical parametric oscillator and directly observe the squeezing of the leading five temporal modes of femtosecond pulsed light. The overlapping spectra of these modes mean that the temporal modes are suitable for use in real-world quantum information applications.

OCIS codes:: 270.6570, 190.7110, 270.5585.
doi: 10.3788/COL201715.092703.

Nonclassical light is not only a fundamental concept in physics but also plays a significant role in quantum information processing applications[1,2]. Recently, considerable research has been devoted to the sources of multimode nonclassical states of light, which will not only be of great value in quantum key sharing and quantum cooperation but will also be an important tool for the expansion of the quantum channel capacity. Recently, continuous-variable (CV) multimode entanglement using a high-dimensional optical parametric oscillator (OPO) was demonstrated in both the frequency domain[3,4] and the spatial domain[5–7]. These multimode sources can also be used to generate compact and scalable multipartite entangled states[8–11], which are essential for quantum communication and computation.

Optical frequency combs, which span thousands of different frequency modes, have the coherence properties of continuous-wave (CW) lasers and the high peak powers of pulsed lasers simultaneously, and have thus become potential tools for temporal multimode nonclassical light generation. Pinel *et al.* experimentally demonstrated a nonclassical frequency comb for the first time in 2012 and obtained amplitude squeezing of −1.2 dB using a synchronously pumped optical parametric oscillator (SPOPO)[12]. Recently, wavelength-multiplexed quantum networks and a quantum spectrometer have been realized based on nonclassical optical frequency combs[13]. In 2013, we observed −2.58 dB phase quadrature squeezing of the TEM_{00} mode by a type-I degenerate SPOPO that was operating below its oscillation threshold[14]. We subsequently obtained amplitude quadrature squeezing of −0.7 dB using an SPOPO that operated in a higher-order transverse mode state in 2016[15,16], which is promising for three-dimensional space-time measurement applications.

In this work, we generated multimode nonclassical frequency comb states using a degenerate type-I SPOPO and directly observed the squeezing of the leading five temporal "supermodes"[17]. Unlike transverse spatial modes[18], these temporal modes are naturally suited to use with existing high-efficiency single-mode fiber networks. In addition, they are insensitive to stationary and slowly varying medium perturbation effects, such as linear dispersion, because of their overlapping spectra, which makes them suitable for use in real-world applications[19].

We consider a degenerate SPOPO with a type-I nonlinear crystal. The Langevin equation of the intracavity signal field is given by:

$$\frac{\mathrm{d}\hat{s}_m}{\mathrm{d}t} = -\gamma_s \hat{s}_m - \gamma_s \sigma \sum_q L_{m,q} \hat{s}_q^{+} + \sqrt{2\gamma_s}\hat{s}_{\mathrm{in},m}. \tag{1}$$

On the right side of this equation, the first term describes the effect of cavity damping, and γ_s is the decay rate. The third term is the input coupling term, which reflects the effects of seed light on the intracavity signal field. The second term describes the parametric interaction that occurs between the two frequency modes. $\hat{s}_k$ are the annihilation operators of the downconversion fields, which are labeled using the integer index k (where $k = m, q$), and $k = 0$ corresponds to the phase-matched mode. $L_{m,q}$ denotes the coupling matrix, which is related to the phase-mismatch factor and the frequency domain profile of the pump and characterizes the coupling strengths s_m and s_q in the nonlinear interaction, and σ is the coupling constant, which is normalized with respect to the CW threshold for a simple-mode OPO[20].

The mode-locked femtosecond pulse laser exports pulse trains of the order of 10^4–10^5 pulses, so the coupling matrix is very large and complex; this means that the parameter downconversion procedure is a highly complex multimode interaction process. The multimode correlations can be simplified into single-mode squeezed states

by the process of Bloch–Messiah reduction[21]; in mathematics, the Bloch–Messiah reduction is the diagonalization of the coupling matrix $L_{m,q}$. The newly obtained eigenbases are temporal modes, which are defined as "supermodes." Additionally, if the pump profile is Gaussian, these supermodes are very close to being a set of modes with orthogonal Hermite–Gauss profiles in the time domain. Analogously, the supermode operators $\hat{s}_k(t)$ satisfy the following equation:

$$\frac{\mathrm{d}}{\mathrm{d}t}\hat{S}_k = -\gamma_s \hat{S}_k - \gamma_s \sigma \Lambda_k \hat{S}_k^{+} + \sqrt{2\gamma_s}\hat{S}_{\mathrm{in},k}, \tag{2}$$

where $\hat{S}_k(t) = \sum_m \mathrm{A}_{k,m}^{+}\hat{s}_m(t)$, $\mathrm{A}_{k,m}$ represents the coupling coefficients of the different frequency modes $\hat{s}_m$, and Λ_k is the eigenvalue of the kth eigenmode of the coupling matrix, where the absolute values decrease with increasing order k[20].

In the Fourier domain, when the input-output relationship is used as a basis, the quadrature noise spectrum of the output signal field of the SPOPO can be expressed as:

$$\delta^2 \tilde{S}_{\mathrm{out},k}^{(\pm)}(\omega) = \frac{\gamma_s^2(1 \mp r\Lambda_k/\Lambda_0)^2 + \omega^2}{\gamma^2(1 \pm r\Lambda_k/\Lambda_0)^2 + \omega^2}, \tag{3}$$

where $\hat{S}^{(+)} = \hat{S} + \hat{S}^T$ and $\hat{S}^{(-)} = -i(\hat{S} - \hat{S}^T)$ represent the amplitudes and the phase quadrature values of the supermodes, respectively. $r = \sigma\Lambda_0$ is the normalized amplitude pumping rate, which is related to both the pump power and the SPOPO oscillation threshold[20]. We can now see that the SPOPO has the characteristics of a general single-mode OPO, including optimal squeezing generation at the threshold and a low analysis frequency; however, the SPOPO output is a set of independently squeezed modes (supermodes), where the squeezing levels are associated with the eigenvalues Λ_k. The squeezing quadrature alternates between successive supermodes because of the alternating sign of the Λ_k values. The squeezing levels are reduced continuously with increasing order k.

As shown in Fig. 1, a Ti:sapphire mode-locked femtosecond pulsed laser produced 130 fs pulse trains that were centered at 850 nm and had a repetition rate of 76 MHz. Its second harmonic, which was centered at 425 nm, served to pump the SPOPO. The SPOPO outputs were measured using a balanced homodyne detection (BHD) scheme[22] with a local oscillator (LO) pulse beam that was produced using a pulse shaper and a mode cleaner (MC). Finally, the differences in the photocurrent fluctuations of the BHD were analyzed using a spectrum analyzer (SA).

The SPOPO consists of two plane mirrors denoted by M1 and M4, two concave mirrors denoted by M2 and M3 with a radius of curvature $R = 30$ cm, and a 350-μm-long nonlinear BiB_3O_6 (BIBO) crystal located centrally between M2 and M3 that allows a reasonable nonlinear efficiency to be maintained. M1 has a high reflectivity at 850 nm and an antireflection coating for 425 nm and is used as the input coupler; M4 has 20% transmission at 850 nm and a high reflectivity at 425 nm and is used as the output coupler. The cavity round-trip length is 3.94 m, which is equal to the resonant cavity length of the laser. The cavity finesse is $F = 25$, which leads to a cavity bandwidth of 3 MHz and an escape efficiency of 79.6%. An 850 nm pulse laser that is synchronized with the pump pulse in both time and space is injected into the SPOPO to act as the seed beam and lock the SPOPO using the Hansch–Couillaud frequency locking technique[23]. The pump power (175 mW) is lower than the SPOPO threshold in our case; simultaneously, the relative phase between the seed and pump beams is locked in the deamplification regime using PZT1.

The pulse shaper with the so-called 4f line[24,25] consists of two diffraction gratings, two lenses with equal focal lengths of $f = 50$ cm, and a programmable 128-pixel spatial light modulator (SLM) in the Fourier plane (i.e., the rear focal plane of the lens). We can arbitrarily manipulate the output pulse shape by loading a suitable function on the SLM. In addition, we placed an MC after the pulse shaper to filter the spatial modes. The MC structure is identical to that of the SPOPO but without the nonlinear crystal.

The simulation results for the pulse shapes of the leading five LOs (i.e., S_0, S_1, S_2, S_3, and S_4) are shown in Fig. 2. Figure 2(a) shows the five different phases that

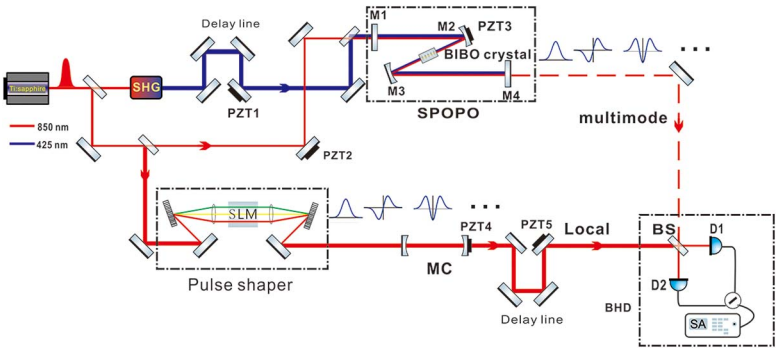

Fig. 1. Experimental setup for the generation and measurement of multimode squeezed frequency comb states. SHG: second harmonic generator; Local: local oscillator.

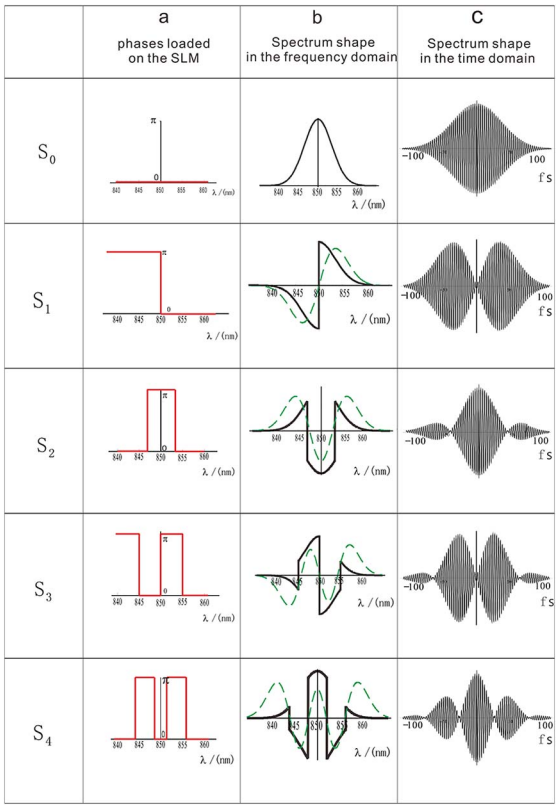

Fig. 2. (Color online) Simulation results for the shaped LO pulses. S_0–S_4 represent the five different modes.

were loaded (red line) on the SLM, with the phases shown from top to bottom corresponding to S_0 to S_4. If nothing is loaded on the SLM, the output pulse shape is identical to the input shape (S_0). In Fig. 2(b), the solid curves (black) indicate the corresponding spectral shapes for the five shaped LOs in the experiment by loading the phase in the corresponding parts of Fig. 2(a). The dotted curves (green) show the standard spectrum shapes for each of the Hermitian–Gaussian polynomial forms. As the results in Fig. 2(b) show, the spectrum shapes of the experimental LOs cannot perfectly match the standard forms. This is because only the phase modulation is loaded on the SLM in the experiment, with no amplitude modulation. In contrast, the spectral widths of the theoretical supermodes increase with the increasing order number ($\Delta\lambda = \sqrt{2k+1} \cdot \Delta\lambda_0$), but the spectrum width of the light that is used to generate the LOs is narrower than that of the higher-order supermodes. Therefore, a higher supermode order number leads to a greater mismatch between the experimental form and the theoretical form. In our case, the degrees of matching between the leading five experimental forms and the corresponding theoretical forms are 100%, 79.8%, 66.0%, 59.0%, and 56.8%. This mismatch will thus cause inefficiency in the squeezing measurement process. Figure 2(c) shows the experimental pulse envelopes of the LOs in the temporal domain.

Using the tailored LOs, we measured the output noise, which was normalized with respect to the shot-noise limit (SNL) at the analysis frequency of 1.2 MHz with a resolution bandwidth (RBW) of 470 kHz and a video bandwidth (VBW) of 620 Hz while the phases (controlled by PZT5) of the LOs were scanned. As shown in Fig. 3, we observed approximately −2.0 dB of amplitude quadrature squeezing for the first supermode, S_0; −1.0 dB of phase quadrature squeezing for the second supermode, S_1; −0.7 dB of amplitude quadrature squeezing for the third supermode, S_2; −0.4 dB of phase quadrature squeezing for the fourth supermode, S_3; −0.1 dB of amplitude quadrature squeezing for the fifth supermode, S_4. We see that the squeezing levels decreased continuously with increasing order k, which agrees well with the theoretical results above. In addition, as shown in Fig. 2, the main factor that causes the inability to match the bandwidths of the higher-order supermodes with the fixed bandwidth of the LO beam also accounts for the reduction in the observed squeezing levels.

The measured squeezing values were also degraded by various inefficiencies in the experiment; we estimate this efficiency to be $\eta_{tol} = \varsigma\eta\xi$, where $\varsigma = 0.99$ is the propagation efficiency, $\eta = 0.86$ is the quantum efficiency of the photodiode (Hamamatsu S5971), and $\xi = 0.94$ is the spatial overlap efficiency between the LO beam and the signal beam. The total estimated detection efficiency is therefore $\eta_{\mathrm{tol}} = 0.80$. From these efficiencies, the inferred squeezing

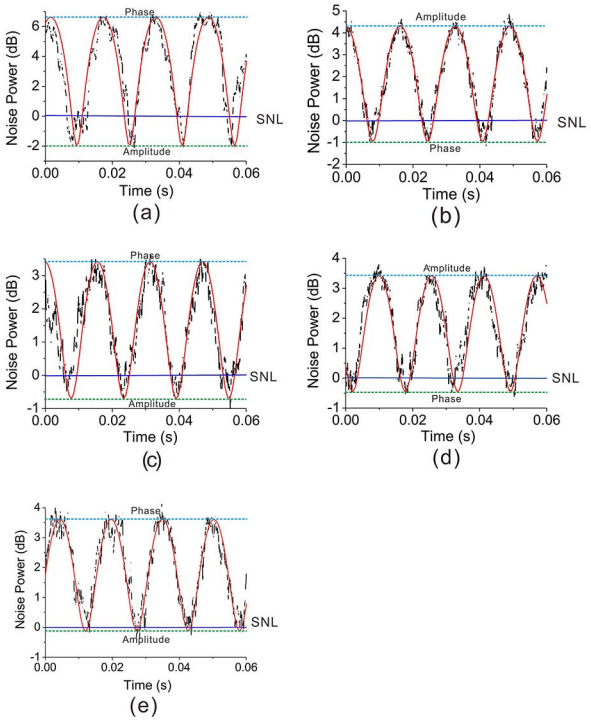

Fig. 3. (Color online) Squeezing traces for the five leading supermodes. In each trace, the blue line represents the SNL, the black dotted line shows the experimental result, the red solid line shows the corresponding fitting curve, and the bottom and top dashed lines indicate the squeezing and anti-squeezing levels, respectively.

levels were −2.69 dB (S_0), −1.25 dB (S_1), −0.90 dB (S_2), −0.52 dB (S_3), and −0.17 dB (S_4).

In conclusion, we experimentally generate the temporal multimode squeezed light of femtosecond frequency combs using a degenerate type-I SPOPO operating below threshold. However, the results cannot represent the upper limit because of additional losses and the narrow spectrum bandwidth of the LO. These temporal multimode squeezed states are promising for use in applications such as quantum measurements of time synchronization and multiplexed quantum communications.

This work was supported by the National Natural Science Foundation of China (Nos. 91536222, 61405108, and 11604189), the Ministry of Science and Technology of China (MOST) (No. 2016YFA0301404), the NSFC Project for Excellent Research Team (No. 61121064), and the University Science and Technology Innovation Project in Shanxi Province (No. 2015103).

References

1. A. Imamoğlu, D. D. Awschalom, G. Burkard, D. P. DiVincenzo, D. Loss, M. Sherwin, and A. Small, Phys. Rev. Lett. **83**, 4204 (1999).
2. S. Hao, X. Deng, Q. Zhang, and X. Su, Chin. Opt. Lett. **13**, 122701 (2015).
3. T. Opatrný, D.-G. Welsch, and W. Vogel, Phys. Rev. A **55**, 1416 (1997).
4. S. Spälter, N. Korolkova, F. König, A. Sizmann, and G. Leuchs, Phys. Rev. Lett. **81**, 786 (1998).
5. B. Chalopin, F. Scazza, C. Fabre, and N. Treps, Opt. Express **19**, 4405 (2011).
6. X. Su, Y. Zhao, S. Hao, X. Jia, C. Xie, and K. Peng, Opt. Lett. **37**, 5178 (2012).
7. K. Liu, J. Guo, C. Cai, S. Guo, and J. Gao, Phys. Rev. Lett. **113**, 170501 (2014).
8. M. Yukawa, R. Ukai, P. van Loock, and A. Furusawa, Phys. Rev. A **78**, 012301 (2008).
9. J. Janousek, K. Wagner, J.-F. Morizur, N. Treps, P. K. Lam, C. C. Harb, and H.-A. Bachor, Nat. Photon. **3**, 399 (2009).
10. S. Armstrong, J.-F. Morizur, J. Janousek, B. Hage, N. Treps, P. K. Lam, and H.-A. Bachor, Nat. Commun. **3**, 1026 (2012).
11. K. Liu, J. Guo, C. Cai, J. Zhang, and J. Gao, Opt. Lett. **41**, 5178 (2016).
12. O. Pinel, P. Jian, R. M. de Araújo, J. Feng, B. Chalopin, C. Fabre, and N. Treps, Phys. Rev. Lett. **108**, 083601 (2012).
13. J. Roslund, R. M. de Araújo, S. Jiang, C. Fabre, and N. Treps, Nat. Photon. **8**, 109 (2014).
14. H. Y. Liu, L. Chen, L. Liu, Y. Ming, K. Liu, J. X. Zhang, and J. R. Gao, Acta Phys. Sin. **62**, 164206 (2013).
15. L. Liu, N. Huo, K. Liu, J. X. Zhang, and J. R. Gao, Acta Sin. Quantum Opt. **20**, 124 (2014).
16. N. Huo, C. Zhou, H. Sun, K. Liu, and J. Gao, Chin. Opt. Lett. **14**, 062702 (2016).
17. G. J. Valcarcel, G. Patera, N. Treps, and C. Fabre, Phys Rev. A **74**, 061801 (2006).
18. J. Wang, Chin. Opt. Lett. **15**, 030005 (2017)
19. B. Brecht, D. V. Reddy, C. Silberhorn, and M. G. Raymer, Phys. Rev. X **5**, 041017 (2015).
20. G. Patera, N. Treps, C. Fabre, and G. J. de Valcárcel, Eur. Phys. J. D **56**, 123 (2010).
21. S. L. Braunstein, Phys. Rev. A **71**, 055801 (2005).
22. K. Liu, S. Z. Cui, H. L. Zhang, J. X. Zhang, and J. R. Gao, Chin. Phys. Lett. **28**, 074211 (2011).
23. T. W. Hansch and B. Couillaud, Opt. Commun. **35**, 441 (1980).
24. A. M. Weiner, D. E. Leaird, J. S. Patel, and J. R. Wullert, IEEE J. Quantum Electron. **28**, 908 (1992).
25. A. Monmayrant, S. Weber, and B. Chatel, J. Phys. B: At. Mol. Opt. Phys. **43**, 103001 (2010).